Pliant Active and Reactive Power Control for Grid-Interactive Converters Under Unbalanced Voltage Dips

Fei Wang, *Student Member, IEEE*, Jorge L. Duarte, *Member, IEEE*, and Marcel A. M. Hendrix, *Member, IEEE*

Abstract—During voltage dips continuous power delivery from distributed generation systems to the grid is desirable for the purpose of grid support. In order to facilitate the control of inverter-based distributed power generation adapted to the expected change of grid requirements, generalized power control strategies based on symmetric-sequence components are proposed in this paper, aiming to manipulate the delivered instantaneous power under unbalanced voltage dips. It is shown that active and reactive power can be independently controlled with two individually adaptable parameters. By changing these parameters, the relative amplitudes of oscillating power can be smoothly regulated, as well as the peak values of three-phase grid currents. As a result, the power control of grid-interactive inverters becomes quite flexible and adaptable to various grid requirements or design constraints. Furthermore, two strategies for simultaneous active and reactive power control are proposed that preserve flexible controllability; an application example is given to illustrate the simplicity and adaptability of the proposed strategies for online optimization control. Finally, experimental results are provided that verify the proposed power control.

Index Terms—Distributed power generation, grid fault, grid-interactive converter, power control, voltage dip.

I. INTRODUCTION

VOLTAGE dips, usually caused by remote grid faults in the power system, are short duration decreases in rms voltage. Most voltage dips are due to unbalanced faults, while balanced voltage dips are relatively rare in practice [1], [2]. Conventionally, a distributed generation (DG) system, as shown in Fig. 1, would be required to disconnect from the grid when voltage dips occur and to reconnect to the grid when faults are cleared. However, this requirement is changing. With the increasing application of renewable energy sources, more and more DG systems actively deliver electricity into the grid. In particular, wind power generation is becoming an important
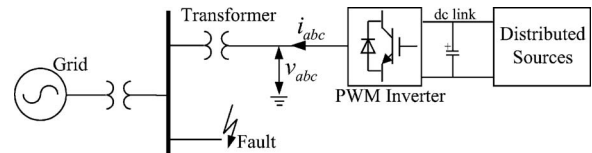
Fig. 1. Single-line diagram of inverter-based DG under grid faults.

electricity source in many countries. Consequently, in order to maintain active power delivery and reactive power support to the grid, grid codes now require wind energy systems to ride through voltage dips without interruption [3], [4]. For the future scenario of a grid with significant DG penetration, it is necessary to investigate the ride-through control of wind turbine systems and other DG systems as well. Disregarding various upstream distributed sources and their controls, this paper will focus on the grid-side DG inverters.

Concerning the control of DG inverters under voltage dips, especially unbalanced situations, two aspects should be noticed. First, fast system dynamics and good reference tracking are necessary. Current controllers must be able to deal with all the symmetric-sequence components and to have fast feedback signals for closed-loop control. Second, in case of unbalanced voltage dips, the employment of different power control strategies, i.e., the generation of reference currents, is also very important. Because this paper mainly concentrates on the second aspect, the control structure of such inverters will be presented in the section dedicated to experimental verifications.

Under unbalanced voltage dips, current reference generation is constrained by tradeoffs. Considering the power electronics converter constraints, a constant dc-link voltage is desirable [5] and [6]. However, a constant dc bus is achieved at the cost of unbalanced grid currents, and this results in a decrease of maximum deliverable power. In [7], a power reducing scheme is used to limit the current during grid faults. However, the effects of the grid currents on the utility side should also be taken into account when assigning reference currents for DG inverters. As presented in [8] and [9], several specific strategies are possible in order to get different power quality levels at the grid connection point in terms of instantaneous power oscillation and current distortion. One of the methods in [8], which is based on instantaneous power theory [10], obtains zero instantaneous power oscillation, but generates distorted grid currents due to the asymmetry of grid voltages. Other methods in [8] lead to sinusoidal output currents. These strategies show flexible control possibilities of DG systems under grid faults. However, they

only cope with specific objectives, such as zero instantaneous active power, balanced current outputs, or unity power factor.

Since voltage dips are as diverse as grid faults, there are always multiple objectives constrained by converters or by grid requirements for grid-fault ride-through control, and these objectives have to be compromised and be adapted under different grid faults, so as to optimize system overall performance. Therefore, a generalized power control strategy, which can be easily adapted to fulfill different objectives under voltage dips, is research area of interest. Starting from the ideas in [8] and [9], this paper proposes generalized active and reactive power control strategies that enable DG inverters to be optimally designed under voltage dips.

This paper is organized as follows. In Section II, instantaneous power calculation is presented along with notation definition. The derivation of proposed strategies for independent active and reactive power control are described in Section III. Then, two strategies for simultaneous active and reactive power control are derived and compared in Section IV, which preserve the adaptive controllability. In Section V, an application example illustrates the simplicity and adaptability of the proposed strategies for on-line optimization control. Finally, experimental verifications of the proposed power control strategies are presented in Section VI.

II. INSTANTANEOUS POWER CALCULATION

To investigate power control strategies, the instantaneous power theory [10], [11] is revisited in this section. Then, instantaneous power calculation based on symmetric sequences is presented, and the notation for the reference current design is defined in the next sections.

A. Instantaneous Power Theory

For a three-phase DG inverter, instantaneous active and reactive power at the grid connection point are given by, respectively,

$$p = \mathbf{v} \cdot \mathbf{i} = v_a i_a + v_b i_b + v_c i_c \qquad (1)$$

$$q = \mathbf{v}_\perp \cdot \mathbf{i} = \frac{1}{\sqrt{3}}[(v_a - v_b)i_c + (v_b - v_c)i_a + (v_c - v_a)i_b] \qquad (2)$$

with

$$\mathbf{v}_\perp = \frac{1}{\sqrt{3}} \begin{bmatrix} 0 & 1 & -1 \\ -1 & 0 & 1 \\ 1 & -1 & 0 \end{bmatrix} \mathbf{v}$$

where $\mathbf{v} = [\, v_a \quad v_b \quad v_c \,]^T$, $\mathbf{i} = [\, i_a \quad i_b \quad i_c \,]^T$, bold symbols represent vectors, and the operator "·" denotes the dot product of vectors. Note that the subscript "$\perp$" is used to represent a vector derived from the matrix transformation in (2), although vectors $\mathbf{v}_\perp$ and $\mathbf{v}$ are orthogonal only when the three-phase components in vector $\mathbf{v}$ are balanced.

B. Symmetric-Sequence-Based Instantaneous Power

Symmetric-sequence transformation is a proven way to decompose unbalanced multiphase quantities [12]. Note that in the experiment, these symmetric-sequence components are detected in the time domain. Consequently, instantaneous quantities for unbalanced abc voltages are represented by

$$\mathbf{v} = \mathbf{v}^+ + \mathbf{v}^- + \mathbf{v}^0 \qquad (3)$$

where $\mathbf{v}^{+,-,0} = [\, v_a^{+,-,0} \quad v_b^{+,-,0} \quad v_c^{+,-,0} \,]^T$, and subscripts "+," "-," and "0" denote positive, negative, and zero sequences, respectively.

Similarly, current quantities can also be represented in terms of symmetric sequences, i.e.,

$$\mathbf{i} = \mathbf{i}^+ + \mathbf{i}^- + \mathbf{i}^0 \qquad (4)$$

where $\mathbf{i}^{+,-,0} = [\, i_a^{+,-,0} \quad i_b^{+,-,0} \quad i_c^{+,-,0} \,]^T$. As a result, the calculation of instantaneous power in (1) and (2) can be rewritten as follows:

$$p = \mathbf{v} \cdot \mathbf{i} = (\mathbf{v}^+ + \mathbf{v}^- + \mathbf{v}^0) \cdot (\mathbf{i}^+ + \mathbf{i}^- + \mathbf{i}^0) \qquad (5)$$

$$q = \mathbf{v}_\perp \cdot \mathbf{i} = (\mathbf{v}_\perp^+ + \mathbf{v}_\perp^- + \mathbf{v}_\perp^0) \cdot (\mathbf{i}^+ + \mathbf{i}^- + \mathbf{i}^0). \qquad (6)$$

With respect to the definitions of the symmetric-sequence vector in (3), corresponding orthogonal vectors in (6) can be derived by using the matrix transformation in (2). Note that $\mathbf{v}_\perp^+$ lags $\mathbf{v}^+$ by 90°, $\mathbf{v}_\perp^-$ leads $\mathbf{v}^-$ by 90°, and $\mathbf{v}_\perp^0$ is always equal to zero. Because the dot products between $\mathbf{i}^0$ and positive-sequence or negative-sequence voltage vectors are also always zero (due to symmetry of the components in $\mathbf{v}^+$ and $\mathbf{v}^-$), (5) and (6) can be simplified by

$$p = \mathbf{v} \cdot \mathbf{i} = (\mathbf{v}^+ + \mathbf{v}^-) \cdot (\mathbf{i}^+ + \mathbf{i}^-) + \mathbf{v}^0 \cdot \mathbf{i}^0 \qquad (7)$$

$$q = \mathbf{v}_\perp \cdot \mathbf{i} = (\mathbf{v}_\perp^+ + \mathbf{v}_\perp^-) \cdot (\mathbf{i}^+ + \mathbf{i}^-). \qquad (8)$$

Because the calculation of instantaneous power and current references is carried out in terms of vectors, it can also be used in other reference frames, simply by substituting the vectors in the abc frame with vectors derived in other frames, for example, the stationary $\alpha\beta\gamma$-reference frame.

In next sections, current control based only on positive-sequence and negative-sequence components is investigated. Because zero-sequence voltages of unbalanced voltage dips do not exist in three-wire systems, nor can they propagate to the secondary side of star-ungrounded or delta-connected transformers in four-wire systems, most case studies only consider positive and negative sequences. Even for unbalanced systems with zero-sequence voltage, four-leg inverter topologies can eliminate zero-sequence current with appropriate control. Simplifying assumptions, we will use:

1) only positive-sequence and negative-sequence currents are present;
2) only fundamental voltages exist, in practice, they can be extracted out;
3) the amplitude of the positive-sequence voltage is higher than the negative sequence one.
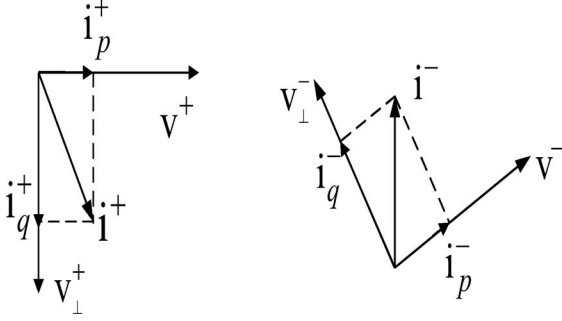
Fig. 2. Decomposition of currents for independent *PQ* control.

III. STRATEGIES FOR INDEPENDENT *PQ* CONTROL

In order to separately analyze the contribution of currents to independent active and reactive power control, sequence currents $\mathbf{i}^{+,-}$ can be decoupled into two orthogonal quantities, i.e., $\mathbf{i}_p^{+,-}$ and $\mathbf{i}_q^{+,-}$, as depicted in Fig. 2. The subscript "p" is related to active power control, and "q" is related to reactive power control.

A. Reactive Power Control

For reactive power control, only $\mathbf{i}_q^+$ and $\mathbf{i}_q^-$ are present, which are defined in phase with $\mathbf{v}_\perp^+$ and $\mathbf{v}_\perp^-$, respectively, in order to generate reactive power only. Rewriting (7) and (8), in terms of $\mathbf{i}_q^+$ and $\mathbf{i}_q^-$, we obtain

$$p = \underbrace{\mathbf{v}^+ \cdot \mathbf{i}_q^- + \mathbf{v}^- \cdot \mathbf{i}_q^+}_{\tilde{p}_{2\omega}} \tag{9}$$

$$q = \underbrace{\mathbf{v}_\perp^+ \cdot \mathbf{i}_q^+}_{Q^+} + \underbrace{\mathbf{v}_\perp^- \cdot \mathbf{i}_q^-}_{Q^-} + \underbrace{\mathbf{v}_\perp^- \cdot \mathbf{i}_q^+ + \mathbf{v}_\perp^+ \cdot \mathbf{i}_q^-}_{\tilde{q}_{2\omega}} \tag{10}$$

where Q^+ and Q^- denote the constant reactive power introduced by positive and negative sequences, respectively, $\tilde{p}_{2\omega}$ represents oscillating active power, and $\tilde{q}_{2\omega}$ oscillating reactive power. It can be found that the two terms of $\tilde{p}_{2\omega}$ are in-phase quantities oscillating at twice the fundamental frequency. A similar property can be found for the two terms of $\tilde{q}_{2\omega}$.

Because oscillating active power can reflect a variation on the dc-link voltage, and high dc voltage variation may cause overvoltage problems, output distortion, or even control instability, it is desirable to eliminate $\tilde{p}_{2\omega}$. On the other hand, the oscillating reactive power $\tilde{q}_{2\omega}$ also causes power losses and operating current rise, and therefore, it is advantageous to mitigate $\tilde{q}_{2\omega}$ as well. A tradeoff between $\tilde{p}_{2\omega}$ and $\tilde{q}_{2\omega}$ is not straightforward and depends on practical requirements. In the following, strategies to achieve controllable oscillating active and reactive power are derived from two considerations.

1) Controllable Oscillating Reactive Power: For a desired level of injection into the grid of reactive power Q, which, for the DG system under consideration, should be determined in advance in agreement with the grid operator by taking also into account the inverter power ratings, the first two terms of (10)

are designed to meet

$$Q = \mathbf{v}_\perp^+ \cdot \mathbf{i}_q^+ + \mathbf{v}_\perp^- \cdot \mathbf{i}_q^-. \tag{11}$$

Since the other two terms of $\tilde{q}_{2\omega}$ in (10) are in-phase quantities, it is convenient that these two terms can easily compensate each other. Therefore, by setting intentionally

$$\mathbf{v}_\perp^+ \cdot \mathbf{i}_q^- = -k_q \mathbf{v}_\perp^- \cdot \mathbf{i}_q^+, \quad 0 \le k_q \le 1 \tag{12}$$

where k_q is a scalar coefficient used as a weighting factor for the elimination of $\tilde{q}_{2\omega}$, and the subscript "q" is related to reactive power (Q) control. After some manipulations, the negative-sequence current $\mathbf{i}_q^-$ is derived from (12) as follows:

$$\mathbf{i}_q^- = \frac{-k_q \mathbf{v}_\perp^+ \cdot \mathbf{i}_q^+}{\left\| \mathbf{v}_\perp^+ \right\|^2} \mathbf{v}_\perp^- \tag{13}$$

where $\left\| \mathbf{v}_\perp^+ \right\|^2 = \left\| \mathbf{v}^+ \right\|^2 = \mathbf{v}^+ \cdot \mathbf{v}^+$, operator "$\| \cdot \|$" means the norm of a vector.

Substituting (13) into (11), and using $\left\| \mathbf{v}_\perp^{+,-} \right\|^2 = \left\| \mathbf{v}^{+,-} \right\|^2$, we obtain

$$Q \left\| \mathbf{v}^+ \right\|^2 = \left(\left\| \mathbf{v}^+ \right\|^2 - k_q \left\| \mathbf{v}^- \right\|^2 \right) \left(\mathbf{v}_\perp^+ \cdot \mathbf{i}_q^+ \right). \tag{14}$$

Then, based on (13) and (14), currents $\mathbf{i}_q^+$ and $\mathbf{i}_q^-$ can be calculated as follows:

$$\mathbf{i}_q^+ = \frac{Q}{\left\| \mathbf{v}^+ \right\|^2 - k_q \left\| \mathbf{v}^- \right\|^2} \mathbf{v}_\perp^+ \tag{15}$$

$$\mathbf{i}_q^- = \frac{-k_q Q}{\left\| \mathbf{v}^+ \right\|^2 - k_q \left\| \mathbf{v}^- \right\|^2} \mathbf{v}_\perp^-. \tag{16}$$

Finally, the total current reference $\mathbf{i}_q^*$ is the sum of $\mathbf{i}_q^+$ and $\mathbf{i}_q^-$, i.e.,

$$\mathbf{i}_q^* = \frac{Q}{\left\| \mathbf{v}^+ \right\|^2 - k_q \left\| \mathbf{v}^- \right\|^2} (\mathbf{v}_\perp^+ - k_q \mathbf{v}_\perp^-), \quad 0 \le k_q \le 1. \tag{17}$$

2) Controllable Oscillating Active Power: Instead of compensating the oscillating reactive power in (10), we can similarly control the oscillating active power $\tilde{p}_{2\omega}$ in (9). For this purpose, negative-sequence currents are imposed to meet

$$\mathbf{v}^+ \cdot \mathbf{i}_q^- = -k_q \mathbf{v}^- \cdot \mathbf{i}_q^+, \quad 0 \le k_q \le 1 \tag{18}$$

where the scalar coefficient k_q is now a weighting factor for the elimination of $\tilde{p}_{2\omega}$. Note that the subscript "q" in k_q remains consistent as used in (12), representing reactive power (Q) control.

By considering that $\mathbf{v}^+ \cdot \mathbf{i}^- = \mathbf{v}_\perp^+ \cdot \mathbf{i}_\perp^-$ (because $\mathbf{v}_\perp^+$ lags $\mathbf{v}^+$ by 90° and $\mathbf{i}_\perp^-$ leads $\mathbf{i}^-$ by 90°), the left side of (18) can be rewritten as follows:

$$\mathbf{v}^+ \cdot \mathbf{i}_q^- = \mathbf{v}_\perp^+ \cdot \mathbf{i}_{q\perp}^- = -k_q \mathbf{v}^- \cdot \mathbf{i}_q^+ \tag{19}$$

where $\mathbf{i}_{q\perp}^-$ denotes the orthogonal vector of $\mathbf{i}_q^-$ according to (2). Then, it follows that

$$\mathbf{i}_{q\perp}^- = \frac{-k_q \mathbf{v}_\perp^+ \cdot \mathbf{i}_q^+}{\left\| \mathbf{v}^+ \right\|^2} \mathbf{v}^-. \tag{20}$$

Hence, the negative-sequence current $\mathbf{i}_q^-$ follows directly from (20) as follows:

$$\mathbf{i}_q^- = \frac{k_q \mathbf{v}_\perp^+ \cdot \mathbf{i}_q^+}{\|\mathbf{v}^+\|^2} \mathbf{v}_\perp^-. \tag{21}$$

Solving (21) and (11), the positive-sequence and negative-sequence currents are derived as follows:

$$\mathbf{i}_q^+ = \frac{Q}{\|\mathbf{v}^+\|^2 + k_q \|\mathbf{v}^-\|^2} \mathbf{v}_\perp^+ \tag{22}$$

$$\mathbf{i}_q^- = \frac{k_q Q}{\|\mathbf{v}^+\|^2 + k_q \|\mathbf{v}^-\|^2} \mathbf{v}_\perp^-. \tag{23}$$

Again, the total current reference $\mathbf{i}_q^*$ is the sum of $\mathbf{i}_q^+$ and $\mathbf{i}_q^-$, i.e.,

$$\mathbf{i}_q^* = \frac{Q}{\|\mathbf{v}^+\|^2 + k_q \|\mathbf{v}^-\|^2} (\mathbf{v}_\perp^+ + k_q \mathbf{v}_\perp^-), \quad 0 \leq k_q \leq 1. \tag{24}$$

3) Merging Strategies [Section III-A.1 and 2]: Simple analysis reveals that (17) and (24) can be put together as follows:

$$\mathbf{i}_q^* = \frac{Q}{\|\mathbf{v}^+\|^2 + k_q \|\mathbf{v}^-\|^2} (\mathbf{v}_\perp^+ + k_q \mathbf{v}_\perp^-), \quad -1 \leq k_q \leq 1. \tag{25}$$

Further, by substituting (25) into (9) and (10), it follows that:

$$p = \frac{Q(1 - k_q)\left(\mathbf{v}_\perp^+ \cdot \mathbf{v}^-\right)}{\|\mathbf{v}^+\|^2 + k_q \|\mathbf{v}^-\|^2} \tag{26}$$

$$q = Q + \frac{Q(1 + k_q)\left(\mathbf{v}_\perp^+ \cdot \mathbf{v}_\perp^-\right)}{\|\mathbf{v}^+\|^2 + k_q \|\mathbf{v}^-\|^2}. \tag{27}$$

It can be seen that the variant terms of (26) and (27), i.e., oscillating active and reactive power, are controlled by the coefficient k_q. These two parts of oscillating power are orthogonal and equal in maximum amplitude.

To observe the controllability of the strategy represented by (25), simulation results are shown in Fig. 3 by sweeping parameter k_q from -1 to 1, where the unbalanced voltage dips are assumed to persist. It is illustrated that either the oscillating active power or the oscillating reactive power can be controlled smoothly and even can be eliminated at the two extremes of the k_q curve. It is pointed out that the strategies presented in [9], namely positive–negative-sequence compensation (PNSC), average active-reactive control (AARC), and balanced positive sequence (BPS) are equivalent to the results of the proposed strategy when k_q equals -1, 1, and 0, respectively. Other than only three specific points, there is a wide choice of possibilities in between with the proposed method, and moreover, strategies from one to another operation point can be simply shifted with the value of the coefficient k_q. This controllable and smooth characteristic allows to enhance system control flexibility and facilitates system optimization. An application example will be presented in Section V.

B. Active Power Control

For a given level of injection into the grid of active power P, which is determined by the power availability of the DG source

and the converter ratings, the current reference for active power control can be derived similarly, as calculated from

$$\mathbf{i}_p^* = \frac{P}{\|\mathbf{v}^+\|^2 + k_p \|\mathbf{v}^-\|^2} (\mathbf{v}^+ + k_p \mathbf{v}^-), \quad -1 \leq k_p \leq 1 \tag{28}$$

where k_p is a similar adjustable coefficient as k_q, but denotes a weighting factor for the elimination of oscillating active or reactive power related to the active power (P) control. Hence, the subscript "p" in k_p denotes active power control. Detailed derivation of (28) has been presented in [13].

IV. STRATEGIES FOR COMBINED *PQ* CONTROL

As already mentioned, some grid codes also require DG systems to contribute with reactive power [3], [4]. For example, with respect to the amplitude drop of voltages, DG systems having agreements with grid operators are expected to deliver both active and reactive power during grid faults. Hence, the reference currents for this case, named $\mathbf{i}_{pq}^*$, can be derived by adding (25) and (28), as expressed by

$$\mathbf{i}_{pq}^* = \mathbf{i}_p^* + \mathbf{i}_q^* = \frac{P}{\|\mathbf{v}^+\|^2 + k_p \|\mathbf{v}^-\|^2} (\mathbf{v}^+ + k_p \mathbf{v}^-)$$
$$+ \frac{Q}{\|\mathbf{v}^+\|^2 + k_q \|\mathbf{v}^-\|^2} (\mathbf{v}_\perp^+ + k_q \mathbf{v}_\perp^-) \tag{29}$$

with $-1 \leq k_p \leq 1, -1 \leq k_q \leq 1$.

It can be seen that there are infinite combinations for (29) with independent coefficients k_p and k_q. This also implicates that the linear controllability benefiting from previous independent power control strategies does not really exist. In order to preserve the controllability, two joint strategies are proposed to simplify (29) by linking the two coefficients. To differ from the symbol k_p used in active power control and k_q used in reactive power control, the coefficient used for combined active and reactive power control in the following is defined as k_{pq}.

A. Joint Strategy With Same-Sign Coefficients

By setting $k_p = k_q = k_{pq}$ in (29), reference current calculation is simplified and rewritten as follows:

$$\mathbf{i}_{pq}^* = \frac{S}{\|\mathbf{v}^+\|^2 + k_{pq} \|\mathbf{v}^-\|^2} \mathbf{R}(\varphi)(\mathbf{v}^+ + k_{pq} \mathbf{v}^-) \tag{30}$$

where $S = \sqrt{P^2 + Q^2}$ is the apparent power and φ is the power factor angle, with

$$\varphi = \cos^{-1}\left(\frac{P}{\sqrt{P^2 + Q^2}}\right). \tag{31}$$

Since the $\alpha\beta$-reference frame is used in the experiment, it can be derived that

$$\mathbf{R}(\varphi) = \begin{bmatrix} \cos\varphi & \sin\varphi \\ -\sin\varphi & \cos\varphi \end{bmatrix}. \tag{32}$$

Note that $\mathbf{R}(\varphi)$ will be different in the *abc*-reference frame.

On the basis of (30), the resulting currents and oscillating powers can now be adjusted by k_{pq}. To help understanding, a vector diagram, representing voltage and current trajectories,
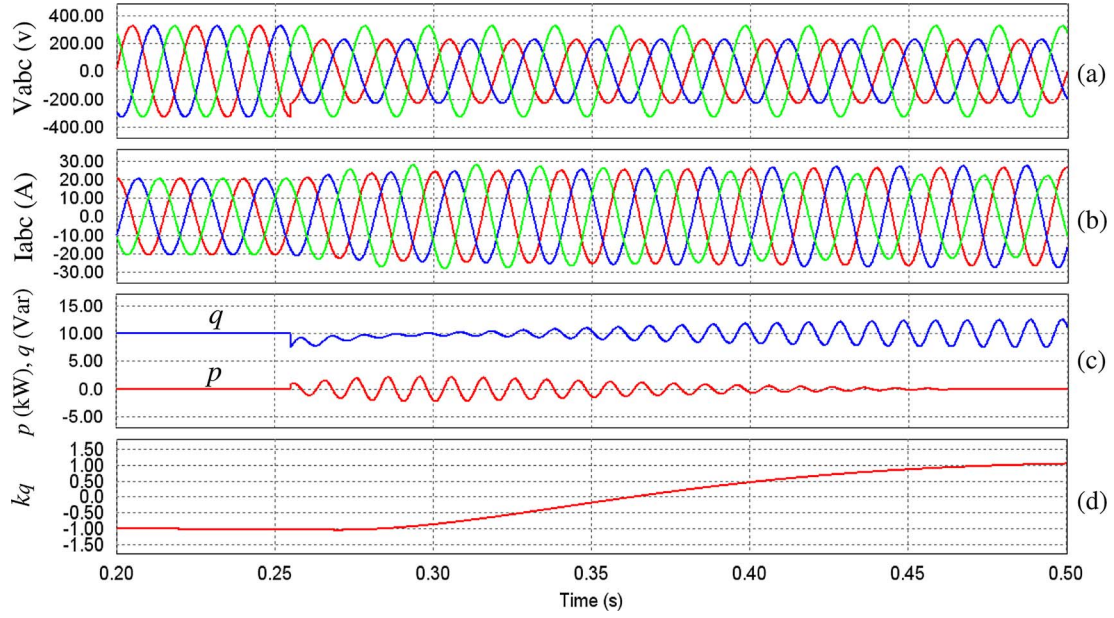
Fig. 3. Simulation results of the proposed reactive power control strategy for 10 kVar power delivery. (a) Phase voltages, where two phases dip to 70% at $t = 0.255$s. (b) Generated current references. (c) Instantaneous active power p and reactive power q. (d) Adjustable coefficient k_q sweeping from -1 to 1.

and the relationship between oscillating powers are plotted with k_{pq} as an adjustable parameter under an unbalanced voltage dip and a certain φ, for instance, 30°.

As shown in Fig. 4(a), when k_{pq} changes from 1 to -1, the length of current vectors changes and reaches a minimum value at $k_{pq} = 0$. In other words, the reference currents given by (30) become balanced when $k_{pq} = 0$. In Fig. 4(b), the amplitudes of the oscillating powers, which are calculated by substituting (30) into (7) and (8), also vary with the change of k_{pq}. Because φ is not 0° or 90°, i.e., active or reactive power is not zero, $\tilde{p}_{2\omega}$ and $\tilde{q}_{2\omega}$ cannot be eliminated, since either active or reactive power delivery always introduces oscillating power at the two extremes of k_{pq}.

B. Joint Strategy With Opposing-Sign Coefficients

By setting $k_p = -k_q = k_{pq}$ in (29), the reference current is represented by

$$\mathbf{i}_{pq}^* = \frac{S\cos\varphi}{\|\mathbf{v}^+\|^2 + k_{pq}\|\mathbf{v}^-\|^2}(\mathbf{v}^+ + k_{pq}\mathbf{v}^-)$$
$$+ \frac{S\sin\varphi}{\|\mathbf{v}^+\|^2 - k_{pq}\|\mathbf{v}^-\|^2}(\mathbf{v}_\perp^+ - k_{pq}\mathbf{v}_\perp^-). \quad (33)$$

Illustrative plots are drawn in Fig. 5. It can be seen from (33) that this joint strategy requires almost twice the computation time of joint strategy A. Fortunately, zero $\tilde{p}_{2\omega}$ or $\tilde{q}_{2\omega}$ can be achieved at the two extremes of k_{pq}, as shown in Fig. 5(b). Similar to joint strategy A, when shifting k_{pq} toward zero, it implies that the length of the current vectors decreases and reaches a minimum value at $k_{pq} = 0$, achieving by this way balanced grid currents. For this value, the current trajectory becomes a circle, as shown in Fig. 5(a).

The main aspects of the two joint strategies are tabulated in Table I. Strategy A can only remove oscillating power when $\varphi = 0°$ or 90°, whereas strategy B allows a more flexible controllability. In summary, the simple adaptive controllability of independent power control strategies is preserved in the joint strategies earlier. This enables DG systems to be optimized under unbalanced voltage dips and make them flexible to meet the upcoming grid codes, which might allow:

1) constant active/reactive power (strategy B);
2) balanced grid currents (strategy A or B);
3) unbalanced currents with limited unbalanced factor [14] (strategy A or B);
4) Average power delivery with limited oscillating power (strategy A or B).

V. APPLICATION EXAMPLE: CONFINED OSCILLATING ACTIVE POWER

To illustrate the simplicity and adaptability of the proposed methods for online optimization control, an application example is given in this section, together with the design procedure. The joint strategy B presented in the previous section is applied to confine the oscillating active power of DG inverters that deliver active power in normal grid conditions and support the grid with reactive power under voltage dips.

First, the control range and regulating directions of k_{pq} should be determined. Considering the power electronics converter constraints, a serious problem for the inverters is the second-order ripple on the dc bus, which reflects to the ac side and creates distorted grid currents during unbalanced voltage dips [15]. Either for facilitating dc-bus voltage control or for minimizing the dc-bus capacitors, it is preferred to make k_{pq} in (33) close to -1, so that the dc voltage variations can be kept very small. However, the maximum deliverable power has to decrease because unbalanced phase currents reduce the operating margin of the inverters. Therefore, for a maximum
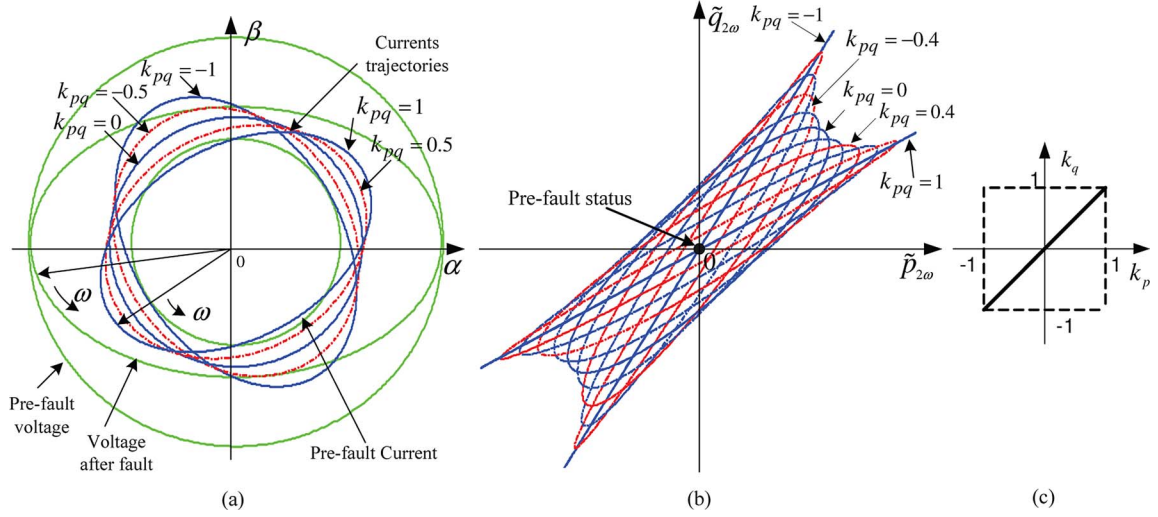
Fig. 4. Graphic representation of (a) grid voltage and current trajectories under unbalanced voltage dips in the stationary frame, and (b) relationship between oscillating active power $\tilde{p}_{2\omega}$ and reactive power $\tilde{q}_{2\omega}$ with k_{pq} as an adjustable parameter under the joint strategy of (c), where $k_p = k_q = k_{pq}$.
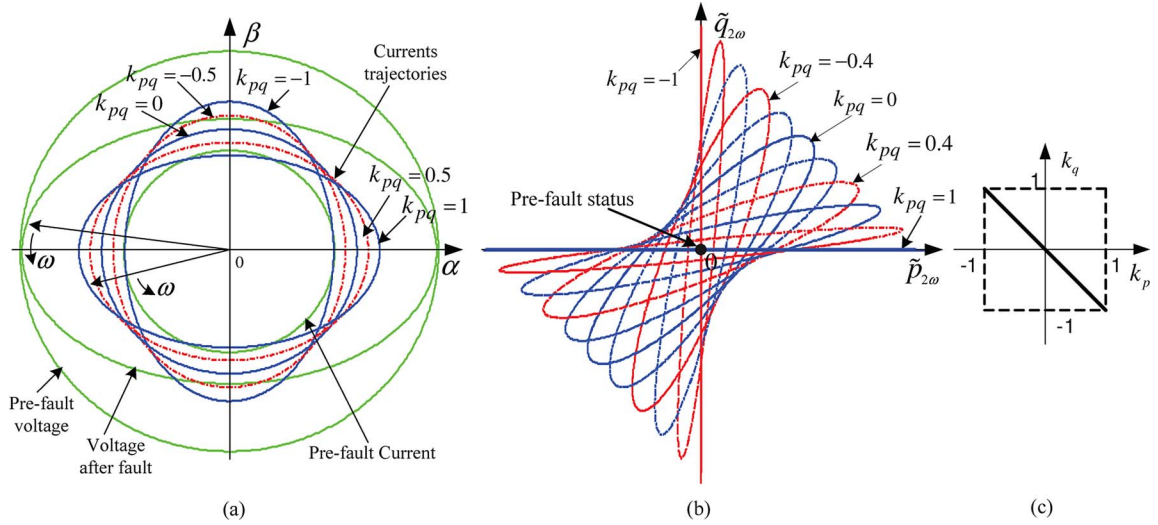

Fig. 5. Graphic representation of (a) grid voltage and current trajectories under unbalanced voltage dips in the stationary frame, and (b) relationship between oscillating active power $\tilde{p}_{2\omega}$ and reactive power $\tilde{q}_{2\omega}$ with k_{pq} as an adjustable parameter under the joint strategy of (c), where $k_p = -k_q = k_{pq}$.

power-tracking system, it is preferable to shift k_{pq} toward zero to get balanced currents as long as the oscillating active power is within a certain limit. It is concluded that the k_{pq} should start from 0, and shifted toward -1 when the amplitude of the oscillating active power is more than a maximum threshold, denoted as $\tilde{p}_{2\omega\_\mathrm{pk}}$.

For a DG inverter, the maximum oscillating active power can be expressed as a function of dc-link capacitance and dc voltage variations, i.e.,

$$\tilde{p}_{2\omega\_\mathrm{pk}} = 2\pi f_1 V_{\mathrm{dc}} C_{\mathrm{dc}} \Delta V_{\mathrm{dc}} \tag{34}$$

where f_1 is the grid fundamental frequency, V_{dc} is the average dc voltage, C_{dc} is the dc-link capacitance, and ΔV_{dc} is the peak-to-peak value of the specified dc voltage variation.

TABLE I
CONTROLLABILITY OF JOINT STRATEGIES

Description	Strategy A	Strategy B
Active power control	yes	yes
Reactive power control	yes	yes
Current symmetry control	yes	yes
Null $\tilde{q}_{2\omega}$ control	no[1]	yes
Null $\tilde{p}_{2\omega}$ control	no[1]	yes

[1] Only possible when $\varphi = 0^0$ or 90^0.

According to (7), the oscillating active power is expressed by

$$\tilde{p}_{2\omega} = \mathbf{v}^+ \cdot \mathbf{i}^- + \mathbf{v}^- \cdot \mathbf{i}^+. \tag{35}$$

Following that, Fig. 6 shows a simple control scheme for regulating k_{pq}. When the oscillating active power is bigger than the $\tilde{p}_{2\omega\_\mathrm{pk}}$, a proportional plus integral (PI) controller ramps up the value of k_{pq} toward -1. Note that the integrator should be reset
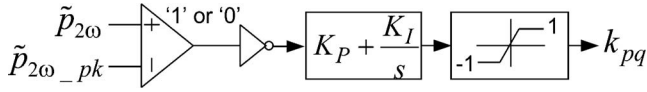
Fig. 6. Control scheme of k_{pq} for confining oscillating active power.

when the grid gets back to normal conditions. Therefore, the oscillating active power will be limited by the adaptive control of k_{pq}, while the output currents are controlled to be as balanced as possible. In similar manners, the proposed strategies can be adapted for optimizing other control objectives.

Note that the oscillating power on account of output filters are not considered. The effects of output inductors are well known, and therefore, are shortly presented here. The instantaneous power control discussed so far has been treated at the grid connection point. When the oscillating power on account of the output inductors cannot be neglected (in case of large and unbalanced currents), the fundamental components of the inverter-bridge output voltages should be used for calculations instead of the grid voltages. Indirect derivation based on grid voltages and currents or direct measurement on the output of inverter bridge can be used to get the required voltages, as presented in [5] and [6].

VI. EXPERIMENTAL VERIFICATIONS

To verify the proposed strategy, experiments are carried out on a laboratory experimental system constructed from a four-leg inverter that is connected to the grid through *LCL* filters, as shown in Fig. 7. The system parameters are listed in Table II, and the grid impedances $Z_{ga,b,c}$ are assumed to be combined with the output inductors. By using a four-leg inverter, zero-sequence currents can be eliminated when the grid has zero-sequence voltages. For the cases, where the zero-sequence voltage of unbalanced grid dips is isolated by transformers, a three-leg inverter can be applied. A 15-kVA three-phase programmable ac power source is used to emulate the unbalanced utility grid, and the distributed source is implemented by a dc power supply. The controller is designed on a dSPACE DS1104 setup by using MATLAB/Simulink.

A. Control Realization

As shown in Fig. 7, the proposed current controller is realized with a double-loop current controller, which consists of an outer control loop with proportional + resonant (PR) controllers for eliminating the steady-state error of the fundamental-frequency currents, and an inner inductor current control loop with simple proportional gain to improve system dynamics and stability. In addition, a feed-forward loop from the grid voltages is used to improve system response to voltage disturbances. Note that the current control used here is only for the laboratory test, but it is not the key point of this paper; other current controllers can also be applied [16]–[18].

The control for both positive-sequence and negative-sequence components would be much too complicated and computation time consuming when conventional PI control with coordinate transformation is used. Therefore, it is preferred to choose a PR

controller in the stationary frame. A quasi-PR controller with a high gain at the fundamental frequency is used

$$G_i(s) = K_p + \frac{2K_r\omega_{br}s}{s^2 + 2\omega_{br}s + \omega_1^2} \tag{36}$$

where K_p is the proportional gain, K_r is the resonant gain, ω_1 denotes the fundamental radian frequency, and ω_{br} the equivalent bandwidth of the resonant controller. A detailed design for the PR controller has been presented in [19] and [20], it is not duplicated here. Through optimizing, the parameters used in the experiment are $K_p = 2$, $K_r = 100$, and $\omega_{br} = 10$ rad/s.

Since the whole controller is designed in the stationary frame, the sequence detection of grid voltages is also realized based on a stationary frame filter cell in the $\alpha\beta$-frame [21]. As shown in Fig. 7, the outputs $v_{\alpha,\beta1}^+$ and $v_{\alpha,\beta1}^-$ denote the α, β quantities of fundamental positive-sequence and negative-sequence voltages, respectively. The basic filter cell can be easily implemented using a multistate-variable structure. A high-performance output can still be achieved under distorted grid voltages. Because of its robustness for small-frequency variations, a phase-locked loop (PLL) is avoided in the experiment, since the ac power supply only emulates the magnitude drop of the grid voltage. Otherwise, a PLL should be added to the filter for adapting to large-frequency changes [21].

Concerning the power factor angle φ, defined in (31), two values are tested in the experiment. First, a slightly modified approach is used here to calculate the angle φ according to the grid code in [3]. Specifically, the DG system should inject at least 2% of the rated current as reactive current for each percentage of the fundamental-sequence voltage dip. Therefore, if the desired angle φ is calculated from

$$\varphi = \sin^{-1}\left(2\frac{|V^+ - V_N|}{V_N}\right) \tag{37}$$

where V_N is nominal voltage amplitude, and $V^+ = \sqrt{(v_{\alpha1}^+)^2 + (v_{\beta1}^+)^2}$ is the positive-sequence voltage amplitude, then the requirements in [3] will be satisfied. Furthermore, it is also required in [3] that a reactive power output of at least 100% of the rated current should be possible when necessary. Hence, also $\varphi = 90°$ will be assigned directly to test a complete range from active to reactive power.

Note that dc-link voltage control is not added here. Usually, a dc-link voltage control loop is included in the control structure, for instance, in a rectifier system [6] or for a wind turbine inverter [7]. The dc bus in the experimental system is only controlled by the dc power supply with a quite low bandwidth to maintain a stable dc bus in an average sense. Since the experiment intends to investigate the effects of the proposed strategies when choosing different k_{pq}, it is convenient to leave out the dc voltage control in order to only observe the performance of the power control strategies.

B. Tests of the Joint Strategies at Specific Operating Points

By shifting the controllable parameter k_{pq} to specific values, the system is tested under unbalanced voltage dips with the joint strategies. In order to capture the transient reaction of the
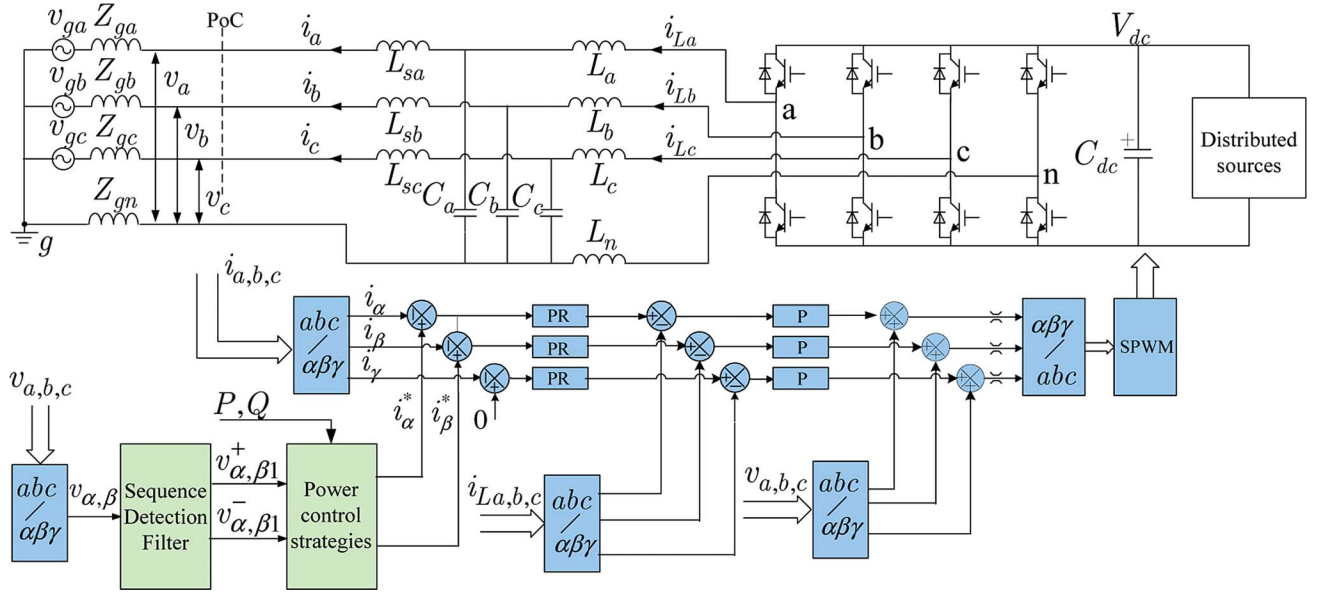
Fig. 7.   Circuit diagram and control structure of experimental four-leg inverter system.

TABLE II
SYSTEM PARAMETERS

Description	Symbol	Value
Output filtering inductor	$L_{sa,b,c}$	2mH
Output filtering capacitor	$C_{a,b,c}$	5μF
Output filtering inductor	$L_{a,b,c}$	2mH
Neutral filtering inductor	L_n	0.67mH
dc-link voltage	V_{dc}	750V
dc-link capacitors	C_{dc}	4400μF
Switching frequency	f_{sw}	16kHz
System rated power	S_{rat}	15kVA
Tested apparent power	S	2500VA
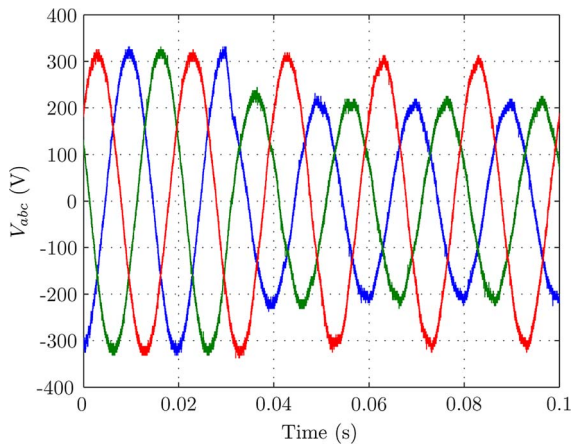
Fig. 8.   Emulated grid voltages to be faulty at $t = 0.03$ s, where two phases dip to 70%.

system, three situations are intentionally tested under equivalent voltage dips.

As shown in Fig. 8, grid voltages are emulated to be faulty at $t = 0.03$ s, where two phases dip to 70%. Consequently, the power factor angle φ derived in the control by (37) is 23° and the corresponding results of joint strategy A are shown in Fig. 9. In order to allow clear observation of the low-order oscillating

power, high-order components are filtered out. It can be seen that the reactive power support starts within half a cycle after voltage dips. As analyzed in Section IV, the instantaneous active and reactive power always have oscillating ripples, and the injected grid currents get balanced only when k_{pq} becomes near to zero. In case φ equals 90° (intentionally imposed), the joint strategy A turns out to be a reactive power control strategy, as expressed by (25). Comparing with the simulation results in Fig. 3 at the point of $k_q = -1$, 0, and 1, it can be seen that the results in Fig. 10 show the same effects on the regulation of oscillating power and reference currents.

Besides, it is noted that the delivered active and reactive power have a certain ramp slope when changing from one average value to the other, and this is because a low-pass filter is used to smooth the output of the power factor angle φ, as calculated in (37). To detect accurate symmetric-sequence voltages under unbalanced and/or distorted voltage dips, the sequence detection filter used in Fig. 7 was designed with a settling time of 20 ms, which copes well with a test condition up to 40% voltage dip. As a result, the outputs from the sequence detection filter after the moment of voltage dips will cause low-frequency ripple on the magnitude value of V^+ in (37), due to unequal amplitudes of $v^+_{\alpha 1}$ and $v^+_{\beta 1}$ at the transient. An extra low-pass filter with also a settling time of 20 ms was used to smooth further the ripple effects on the power factor angle. For other unbalance conditions, the settling time of the sequence detection filter and the low-pass filter should be optimized. Other fast detection techniques [22] can also be used, thereby improving the design.

Under the same test conditions, experimental results are also measured for joint strategy B. As shown in Fig. 11, nearly zero oscillating reactive and active power are achieved at $k_{pq} = 1$ and -1, respectively. When $k_{pq} = 0$, the results of joint strategy B are the same as the results of joint strategy A, since both joint strategies only depend on positive-sequence components in this case. The results with $\varphi = 90°$ are given in Fig. 12. Comparing with the results in Fig. 10 of joint strategies A, it is clear that the
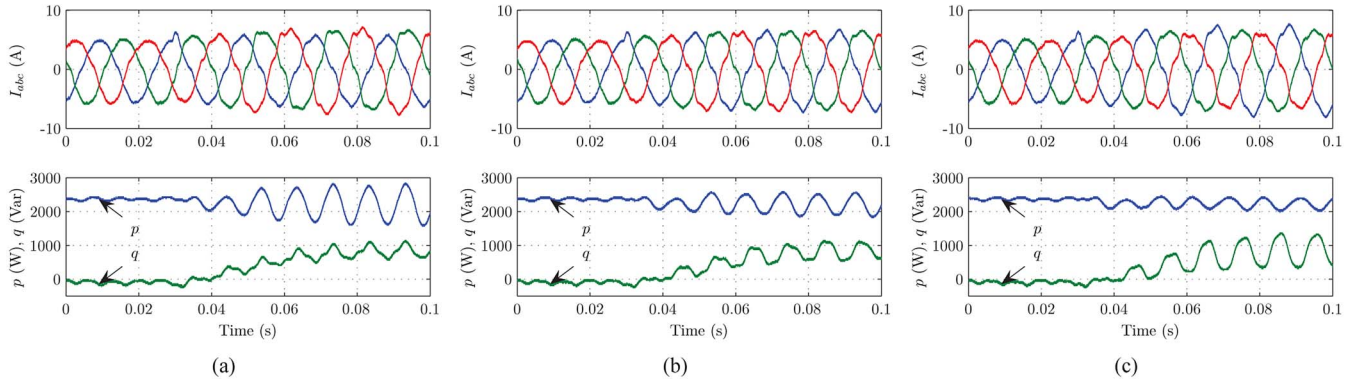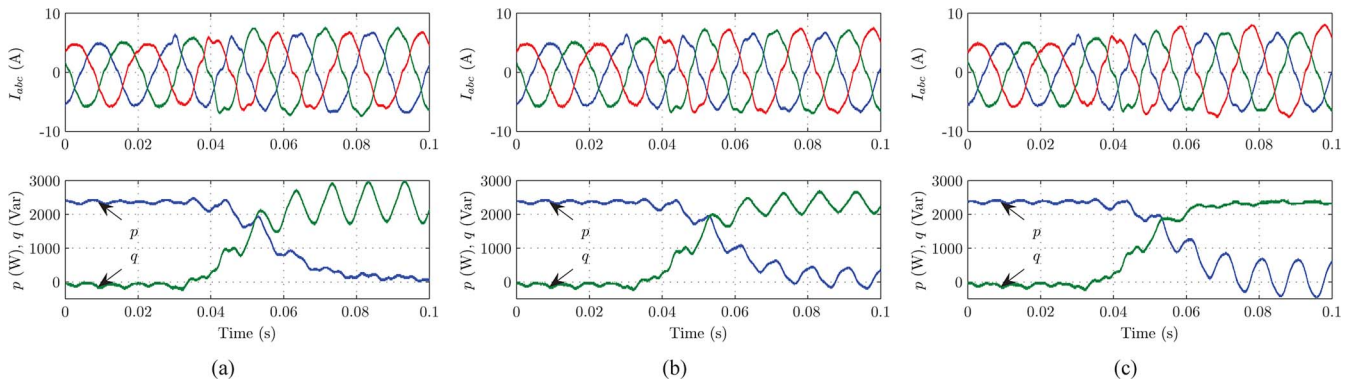
Fig. 9. Experimental results of the joint strategy A with k_{pq} set to (a) 1, (b) 0, and (c) -1, where the waveforms from the top to down are injected currents, instantaneous active power p, and reactive power q when $\varphi = 23°$.

Fig. 10. Experimental results of the joint strategy A with k_{pq} set to (a) 1, (b) 0, and (c) -1, where the waveforms from the top to down are injected currents, instantaneous active power p, and reactive power q when $\varphi = 90°$.
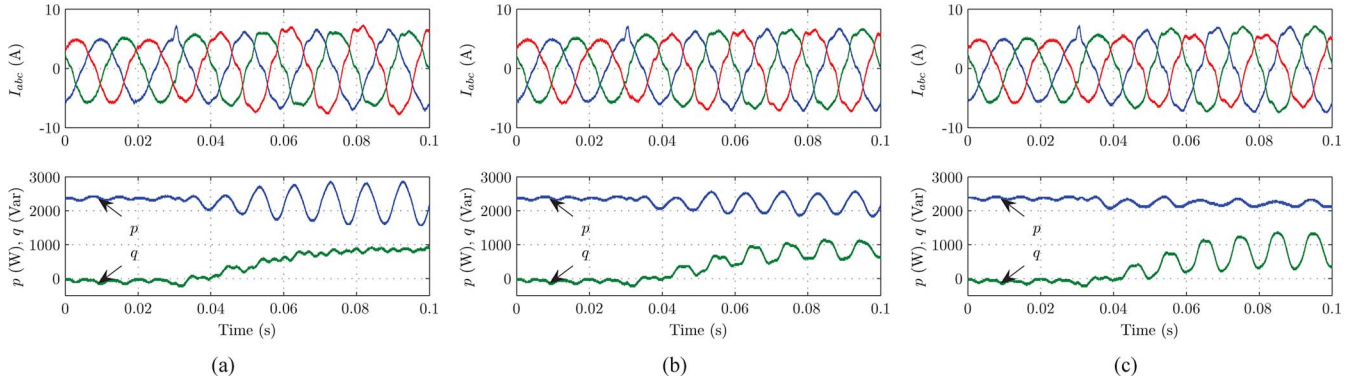

Fig. 11. Experimental results of the joint strategy B with k_{pq} set to (a) 1, (b) 0, and (c) -1, where the waveforms from the top to down are injected currents, instantaneous active power p, and reactive power q when $\varphi = 23°$.

joint strategies with opposite signs of k_{pq} turn out to produce the same results.

It is noted that the grid currents are slightly distorted especially after a grid fault. There are two reasons that cause the low-frequency harmonic currents. The first one is the dead-time effect of the insulated gate bipolar transistor inverter bridges used in the laboratory system. Harmonic distortion is introduced into the output voltage of the inverter when the dead time is large to a certain extent (in this paper, a fixed dead time reaches 4% of the switching period), resulting in distorted currents through small grid impedances. This distortion will be less when increasing the fundamental currents. The second reason is the dc-link voltage variations. In the experimental verifications, a dc-link voltage control was not implemented in order to allow observing the behavior of the power control strategies. In this case, variations are present in the dc voltage when changing the delivered power after grid faults and/or when oscillating active power exists. Therefore, the voltage variations reflect to the grid side, leading to low-frequency current harmonics.
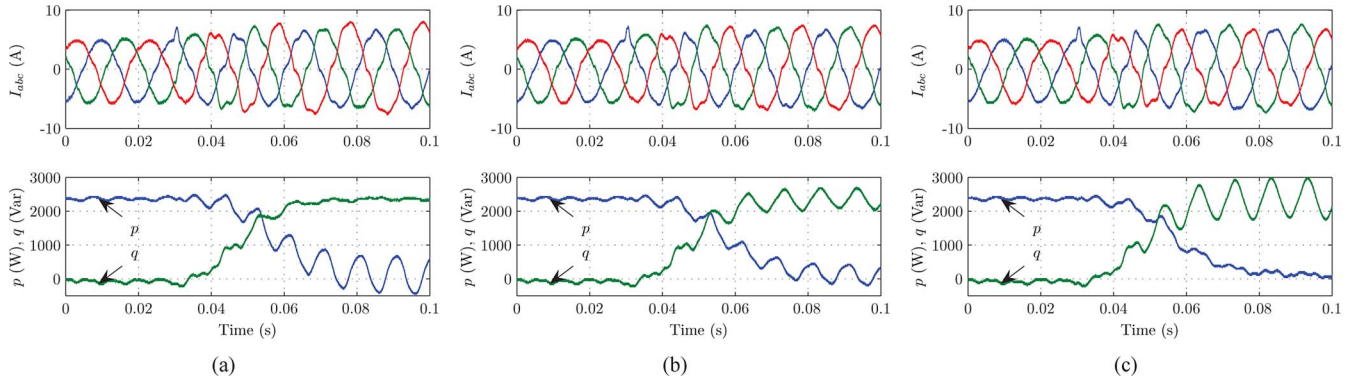
Fig. 12.   Experimental results of the joint strategy B with k_{pq} set to (a) 1, (b) 0, and (c) -1, where the waveforms from the top to down are injected currents, instantaneous active power p, and reactive power q when $\varphi = 90°$.
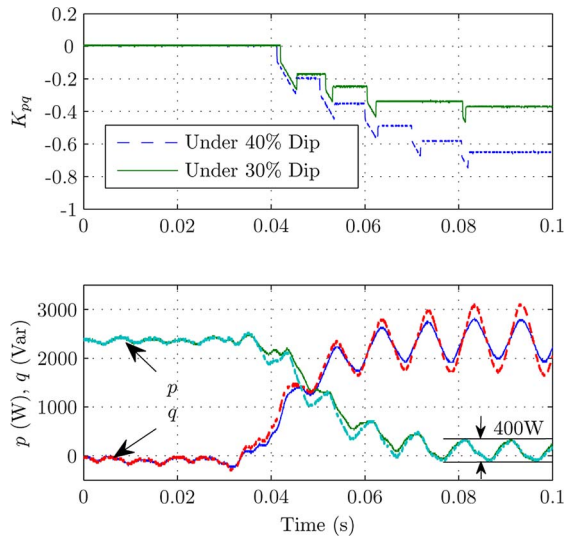

Fig. 13.   Measured waveforms of regulated coefficient k_{pq}, instantaneous active power p and reactive power q.

C. Test of Adaptive Control With Joint Strategy B

Next, the joint strategy B is applied to confine the oscillating active power of the inverter under unbalanced voltage dips with the control scheme presented in Section V. The PI parameters are $K_P = 0.1$ and $K_I = 50\,\text{s}^{-1}$. Because the tested power level is around 2.5 kW, a value of 200 W is assigned to $\tilde{p}_{2\omega\_\text{pk}}$ as the peak limit of oscillating active power, instead of calculating it from (34).

Under the same test conditions as for Fig. 12, with $\varphi = 90°$ and the same phase voltage dip shown in Fig. 8, two levels of voltage dips (30% and 40% dips) are emulated to test the adaptive control of k_{pq}. Measured waveforms are shown in Fig. 13, where the coefficient k_{pq} shifts toward -1 so as to confine the oscillating active power. The deeper the voltage dips, the smaller the k_{pq}. It can be seen that the oscillating components of the active power under two voltage dips are limited below the set point. As a result, the oscillating reactive power under 40% voltage dip is larger than the one under 30% voltage dip.
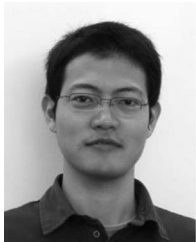
VII. CONCLUSION

This paper has proposed methods for independent active and reactive power control of DG inverters operating under unbalanced voltage dips. The impact of symmetric-sequence components on the instantaneous power and the interactions between symmetric sequences have been explained in detail. Furthermore, for simultaneous control of active and reactive power, two joint strategies have been proposed, yielding an adaptive controllability that can cope with multiple constraints in practical applications. Application examples together with experimental results have been given, which verify the validity of the proposed ideas.

REFERENCES

[1] M. F. McGranaghan, D. R. Mueller, and M. J. Samotyj, "Voltage sags in industrial systems," *IEEE Trans. Ind. Appl.*, vol. 29, no. 2, pp. 397–403, Mar./Apr. 1993.

[2] L. Zhang and M. H. J. Bollen, "Characteristic of voltage dips (sags) in power systems," *IEEE Trans. Power Del.*, vol. 15, no. 2, pp. 827–832, Apr. 2000.

[3] *Grid Code for High and Extra High Voltage*, E.ON Netz Gmbh Std. Bayreuth Germany, 2006. Available: http://www.eon.com.

[4] *The Grid Code*, National Grid Electricity Transmission Std. London, U.K., 2008. Available: http://www.nationalgrid.com/uk.

[5] Y. Suh and T. A. Lipo, "A control scheme in hybrid synchronous-stationary frame for PWM AC/DC converter under generalized unbalanced operating conditions," *IEEE Trans. Ind. Appl.*, vol. 42, no. 3, pp. 825–835, May/Jun. 2006.

[6] B. Yin, R. Oruganti, S. Panda, and A. Bhat, "An output-power-control strategy for a three-phase PWM rectifier under unbalanced supply conditions," *IEEE Trans. Ind. Electron.*, vol. 55, no. 5, pp. 2140–2151, May 2008.

[7] H. Chong, R. Li, and J. Bumby, "Unbalanced-grid-fault ride-through control for a wind turbine inverter," *IEEE Trans. Ind. Appl.*, vol. 44, no. 3, pp. 845–856, May/Jun. 2008.

[8] P. Rodriguez, A. V. Timbus, R. Teodorescu, M. Liserre, and F. Blaabjerg, "Flexible active power control of distributed power generation systems during grid faults," *IEEE Trans. Ind. Electron.*, vol. 54, no. 5, pp. 2583–2592, Oct. 2007.

[9] P. Rodriguez, A. V. Timbus, R. Teodorescu, M. Liserre, and F. Blaabjerg, "Reactive power control for improving wind turbine system behavior under grid faults," *IEEE Trans. Power Electron.*, vol. 24, no. 7, pp. 1798–1801, Jul. 2009.

[10] H. Akagi, E. H. Watanabe, and M. Aredes, *Instantaneous Power Theory and Applications to Power Conditioning*.   Piscataway, NJ: IEEE Press, 2007.

[11] F. Z. Peng and J. -S. Lai, "Generalized instantaneous reactive power theory for three-phase power systems," *IEEE Trans. Instrum. Meas.*, vol. 45, no. 1, pp. 293–297, Feb. 1996.

[12] P. M. Andersson, *Analysis of Faulted Power Systems*. New York: IEEE Press, 1995.

[13] F. Wang, J. Duarte, and M. Hendrix, "Active power control strategies for inverter-based distributed power generation adapted to grid-fault ride-through requirements," in *Proc. EPE*, 2009, pp. 1–10.

[14] A. Jouanne and B. Banerjee, "Assessment of voltage unbalance," *IEEE Trans. Power Del.*, vol. 16, no. 4, pp. 782–790, Oct. 2001.

[15] X. H. Wu, S. K. Panda, and J. X. Xu, "Analysis of the instantaneous power flow for three-phase PWM boost rectifier under unbalanced supply voltage conditions," *IEEE Trans. Power Electron.*, vol. 23, no. 4, pp. 1679–1691, Jul. 2008.

[16] A. Timbus, M. Liserre, R. Teodorescu, P. Rodriguez, and F. Blaabjerg, "Evaluation of current controllers for distributed power geneartion systems," *IEEE Trans. Power Electron.*, vol. 24, no. 3, pp. 654–663, Mar. 2009.

[17] E. Twining and D. G. Holmes, "Grid current regulation of a three-phase voltage source inverter with an LCL input filter," *IEEE Trans. Power Electron.*, vol. 18, no. 3, pp. 888–895, May 2003.

[18] I. J. Gabe, V. F. Montagner, and H. Pinheiro, "Design and implementation of a robust current controller for VSI connected to the grid through an LCL filter," *IEEE Trans. Power Electron.*, vol. 24, no. 6, pp. 1444–1452, Jun. 2009.

[19] D. Zmood and D. Holmes, "Stationary frame current regulation of PWM inverters with zero steady-state error," *IEEE Trans. Power Electron.*, vol. 18, no. 3, pp. 814–822, May 2003.

[20] R. Teodorescu, F. Blaabjerg, M. Liserre, and P. C. Loh, "Proportional-resonant controllers and filters for grid-connected voltage-source converters," *IEE Proc.-Electr. Power Appl.*, vol. 153, no. 5, pp. 750–762, Sep. 2006.

[21] F. Wang, J. Duarte, and M. Hendrix, "High performance stationary frame filters for symmetrical sequences or harmonics separation under a variety of grid conditions," in *Proc. IEEE APEC*, 2009, pp. 1570–1576.

[22] D. Yazdani, M. Mojiri, A. Bakhshai, and G. Joos, "A fast and accurate synchronization technique for extraction of symmetrical components," *IEEE Trans. Power Electron.*, vol. 24, no. 3, pp. 674–684, Mar. 2009.

Jorge L. Duarte (M'00) received the M.Sc. degree from the University of Rio de Janeiro, Rio de Janeiro, Brazil, in 1980, and the Dr.-Ing. degree from the Institut National Polytechnique de Lorraine, Nancy, France, in 1985.

In 1989, he was a Research Engineer at Philips Lighting Central Development Laboratory. Since 1990, he has been with the Group of Electromechanics and Power Electronics, Eindhoven University of Technology, Eindhoven, The Netherlands, as a member of the Academic Staff. Since October 2000, he has been a Consultant Engineer on a regular basis at high-tech industries around Eindhoven. In 2008, he was an Invited Lecturer with the Zhejiang University, Hangzhou, China. He has authored or coauthored more than 100 technical papers. He holds six patents. His current research interests include modeling, simulation, and design optimization of power electronic systems.

Marcel A. M. Hendrix (M'98) received the M.Sc. degree in electronic circuit design from the Eindhoven University of Technology (TU/e), Eindhoven, The Netherlands, in 1981.

He is currently a Senior Principal Engineer at Philips Lighting, Eindhoven. In 1983, he joined Philips Lighting, Eindhoven, where he was engaged in the Predevelopment Laboratory, Business Group Lighting Electronics and Gear for the design and specification of switched-power supplies for both low- and high-pressure gas-discharge lamps. In July 1998, he was a part-time Professor with the Electromechanics and Power Electronics Group, TU/e, where he teaches design-oriented courses in power electronics below 2000 W. His current research interests include cost function-based simulation and sampled data, nonlinear modeling, real-time programming, and embedded control.

Fei Wang (S'07) received the B.Sc. degree in electrical engineering and the M.Sc. degree in power electronics from Zhejiang University, Hangzhou, China, in 2002 and 2005, and the Ph.D. degree from the Eindhoven University of Technology (TU/e), Eindhoven, The Netherlands, in 2010.

From April 2005 to December 2006, he was with Philips Lighting Electronics Global Development Center, Shanghai, China. He is currently an Assistant Professor at the College of Mechatronics and Automation, Shanghai University. His current research interests include distributed power generation, microgrid, and power quality.